RESEARCH PAPER

PCCP
www.rsc.org/pccp

Electrochemical reactivity in nanoscale domains: O_2 reduction on a fullerene modified gold surface

Akiyoshi Kuzume,[a] Enrique Herrero,[b] Juan M. Feliu,[b] Elisabet Ahlberg,[c] Richard J. Nichols[a] and David J. Schiffrin*[a]

[a] *Centre for Nanoscale Science, Department of Chemistry, University of Liverpool, Liverpool, UK L69 7ZD. E-mail: d.j.schiffrin@liv.ac.uk; Fax: +44-151-794-3588; Tel: +44-151-794-3574*

[b] *Departamento de Química-Física, Universidad de Alicante, Apd. 99, E-03080 Alicante, Spain*

[c] *Department of Chemistry, University of Göteborg, S-412 96 Göteborg, Sweden*

Received 26th November 2004, Accepted 25th January 2005
First published as an Advance Article on the web 7th February 2005

Fullerene is strongly adsorbed on both single crystal and polycrystalline gold surfaces and its specific adsorption resulted in the formation of high coverage large hexagonal rafts with strong interactions between the adsorbed fullerene molecules and the Au substrate. The oxygen reduction reaction (ORR) was investigated on these surfaces to determine their influence on the reduction mechanism. Oxygen reduction did not take place on the fullerene overlayer but proceeded on the sub-nanometer sized exposed pockets of the underlying Au substrate. Reduction at these confined sites produces hydrogen peroxide selectively. This effect is ascribed to the blocking action, or so-called "third body effect", of the adsorbed fullerene molecules, which do not display electrocatalytic properties for oxygen reduction.

1. Introduction

Carbon has been extensively used in electrochemical studies due to its inertness and the irreversibility of the hydrogen evolution reaction on this material.[1] In addition, the presence of surface functional groups can lead to specific chemisorption and to the formation of strong covalent bonds with a variety of organic compounds, thus providing a convenient substrate for modification chemistry.[2] However, its variable interfacial morphology and rich chemistry give rise to irreproducibility in electron transfer kinetics measurements.[3,4] Glassy carbon (GC), although displaying a range of surface sites of different reactivity, has been extensively used as an electrode material since it is mechanically strong, non-porous and chemically stable in electrochemical experiments. In contrast, highly ordered pyrolytic graphite (HOPG), although having a well-defined hybridised carbon sp^2 leading to a surface with parallel sheets of hexagonal rings is easily damaged. Fullerene (C_{60}) has not been used specifically as an electrocatalytic material and less attention has been paid to its application as a site for electrochemical electron transfer reactions, and for this reason it was the subject of the present investigation.

Fullerene has attracted much attention since its discovery in 1985 [5] because of its characteristic symmetry and unique properties. For instance, fullerene has eight different redox states;[6] it has a "distorted" (non-planar) structure compared with graphitic carbon and this distortion may lead to new catalytic properties. Fullerene also shows unusual magnetic properties[7] and displays superconductivity when doped with alkali metals.[8] The formation of well-ordered fullerene monolayer and multilayers on metal surfaces by sublimation in vacuum has been widely investigated on a range of substrates (Au, Ag, Cu Si, Ge and GaAs).[9–13] Altman and Colton[9] used STM to investigate the mechanism of fullerene monolayer formation on Au(111) and demonstrated that nucleation starts at step sites separating narrow terraces, followed by film growth on the terraces. A recent study on high index Au single crystal surfaces has shown that fullerene overlayers have a high adaptability to the structure of the underlying substrate and form well-ordered hexagonal and/or quasi hexagonal monolayers with nearest neighbour distances between 1.0 and 1.1 nm.[13] The ease of formation of well-defined fullerene monolayers on Au makes this electrode material ideally suited to investigate the electrocatalytic properties of fullerene.

There is a significant difference between the electrochemistry of fullerene in aqueous solvents and non-aqueous electrolytes. For the former, well-defined redox properties of the different fullerene anions are observed[6] which are absent for the latter. Due to the insolubility of fullerene in aqueous electrolytes, its electrochemical properties have been studied at drop cast films forming multilayers on HOPG, platinum and gold electrodes. These films can be electrochemically reduced in solutions of aqueous alkali metal hydroxides[14–16] to yield conducting layers. It has been proposed that the irreversible transformation observed after reduction corresponds to the intercalation of the cation within the fullerene lattice.[17] The presence of fullerene multilayers inhibits electron transfer for ascorbic acid,[16] the complex between iron and 1,2-cyclohexyldinitrilo tetraacetate,[16] the [Fe(III) EDTA]$^-$ complex,[14] the reduction of cytochrome c [18] and the oxidation of hexacyanoferrate(II).[18] Similar results were observed for electrodes coated with fullerene in acetonitrile solutions.[19] Inhibition of electron transfer reactions caused by this modification of the electrode surfaces was also observed for the oxidation and reduction of several organic compounds.

The reaction chosen for the present studies was the oxygen reduction reaction (ORR), which is important because of its central role in electrochemical energy conversion. This reaction has been investigated extensively and detailed models rationalising the mechanism and complex kinetics on Au surfaces have been previously discussed.[20–26] Although there is no direct spectroscopic identification either of the sites where the ORR takes place or of the configuration of adsorbed oxygen, three possible adsorption models derived from the known coordination chemistry of oxygen have been proposed.[22,27] One is based on end-on adsorption through a σ-bond between oxygen and a

DOI: 10.1039/b417928p

d_{z^2} orbital of the metal forming an adsorbed superoxide. This can then accept a second electron to form hydrogen peroxide (Pauling model). The second model invokes the formation of a μ-peroxo species resulting in a two-fold bridge adsorption of oxygen (Yeager model).[28] Bond breaking then proceeds leading to a four-electron transfer process to give water as the final product.[29] In the third model, oxygen shows side-on coordination and interacts with a single substrate atom *via* two bonds formed mainly between a π orbital of the oxygen molecule and an empty d_{z^2} orbital on the metal surface atom. π back-bonding from the partially filled d_{xy} or d_{yz} orbitals of the metal to the antibonding π* orbital on O_2 contributes to the stability of the surface complex formed (Griffith model).[30] Side-on coordination has been further analysed more recently using quantum chemical calculations.[29]

Recent advances in the study of the reduction of O_2 have focused on the dependence of the reaction mechanism on surface structure[23–26] and anion adsorption.[26] The mechanism on Au is strongly structure-dependent, especially in alkaline and neutral solutions; on Au(111) and Au(110) it follows a two-electron transfer sequence producing hydrogen peroxide:

$$O_2 + H^+ + 2e^- \rightarrow HO_2^- \qquad \text{(I)}$$

while on Au(100) a four-electron transfer process takes place to produce water:

$$O_2 + 4H^+ + 4e^- \rightarrow 2H_2O \qquad \text{(II)}$$

This crystallographic dependence of the reduction mechanism is due to the role of adsorbed hydroxide and/or hydroperoxyl groups, which catalyse further reduction of peroxide to water.[23–26] In the case of polycrystalline Au, the number of electrons transferred per oxygen molecule is between two and four, presumably due to peroxide reactivity on the different exposed planes.

The aim of the present work is to investigate structural and electrocatalytic effects of fullerene monolayers adsorbed on Au on the kinetics of the ORR in order to determine the influence of fullerene in oxygen reduction electrocatalysis.

2. Experimental

The fullerene overlayers were prepared by adsorption from toluene solutions, as previously described.[13] The adsorbed layer was characterised by ellipsometry, X-ray photoelectron spectroscopy (XPS), copper underpotential deposition (Cu UPD) and *ex situ* scanning tunnelling microscopy (STM). Au(111) and Au(100) electrodes for Cu UPD and STM studies were prepared from small beads obtained by fusion of a 0.5 mm diameter Au wire (99.999% Alfa Aesar). The beads (2 mm in diameter) were oriented, cut and polished according to Clavilier's technique.[31] For ellipsometry and XPS measurements, Au films evaporated on glass (250 nm nominal thickness Au film on 11 × 11 mm glass with a *ca.* 2 nm chromium adhesion layer, Arrandee™) were used. These films had mainly a Au(111) orientation. Other experimental details have been described elsewhere.[13]

Ellipsometry measurements to evaluate the thickness of the adsorbed fullerene layer were carried out with a L126B ellipsometer (Gaertner Scientific Corporation) operating with a helium–neon laser (632.8 nm) at an angle of incidence of 70°. A value for the refractive index of fullerene of 2.05 was calculated from the carbon–carbon bond molar refractivity and used in the thickness calculations.[32] The reported values represent the average of at least ten measurements taken at ten different locations on the same sample. The film thickness was calculated from the ellipsometric angles Δ and Ψ using commercial software.[33]

XPS spectra were obtained with a Scienta ESCA300 spectrometer (Daresbury Laboratory, UK). This employs a monochromatic Al Kα X-ray source ($h\nu$ = 1486.7 eV), high transmission electron optics and a multichannel detector. The geometry of the X-ray source, sample manipulator and electrostatic lens allows the use of a low take-off angle, θ. The enhanced sensitivity at low θ is ideal for studying the uppermost surface of a thin film sample. The angular acceptance of the ESCA300 input lens varies with the kinetic energy of the photoelectrons, pass energy and slit-width setting of the spectrometer. For C1*s* photoelectrons and the typical high-energy resolution settings used in this work, θ was 20°; a slit-width of 0.8 mm was employed. The spectra were referenced to the Au $4f_{7/2}$ line at 84.0 eV obtained from a clean Au sample. The Au(111) surface for XPS measurement was cleaned by argon sputtering for 5 min prior to each measurement.

Cu UPD was used to probe the coverage by adsorbed fullerene, which was calculated from the charge under the Cu UPD voltammogram since adsorption of Cu takes place on the free Au domains.[13] The fullerene overlayer was attached on the Au surface by immersion for 1 min in a 1.0 mmol dm^{-3} toluene solution of fullerene.[13]

Oxygen reduction was studied with a rotating disc electrode (RDE) in 0.1 mol dm^{-3} KOH aqueous solution saturated with oxygen. An Au RDE (EDI 101 RDE, Radiometer, Copenhagen) with a disk area of 0.196 cm^2 was employed. The electrode was polished with alumina (1.0, 0.3 and 0.05 μm diameter, Buehler), then rinsed thoroughly with MilliQ® water, followed by sonication to remove any attached alumina. This procedure was repeated before any electrochemical measurements were carried out. The potential was controlled with an Autolab® potentiostat PGSTAT20 (Eco Chemie B. V., The Netherlands) using appropriate software supplied by the manufacturer (General Purpose Electrochemical Software). The counter electrode was a platinum wire and a saturated calomel electrode (SCE) and a reversible hydrogen electrode (RHE) were used as references. All the potentials reported have been referenced to the SCE. Potassium hydroxide (BDH, AnalaR grade) was used as received. MilliQ® water (Millipore, Inc.) was used throughout and electrochemical measurements were performed at room temperature (22 ± 2 °C).

3. Results and discussion

3.1. Characterisation of the fullerene overlayer

Fig. 1 shows an STM image of fullerene adsorbed on a Au(111) surface. The adsorbed film shows a hexagonal close-packed structure with a spacing of 0.99 ± 0.05 nm between nearest neighbours. This result is consistent with previous observations for films obtained using other techniques such as sublimation in vacuum, the Langmuir–Blodgett method and by simple casting from organic solvents.[34–36] The ellipsometric thickness measured was 0.93 ± 0.05 nm, supporting the STM evidence for full coverage of gold surfaces by adsorbed fullerene.

Cu UPD voltammetric measurements provide a sensitive method for probing the coverage of the adlayers.[13,37] The coulometric charge for Cu UPD was calculated from the voltammogram for Au(111) in the absence and presence of adsorbed fullerene. The Cu UPD value obtained for a bare Au

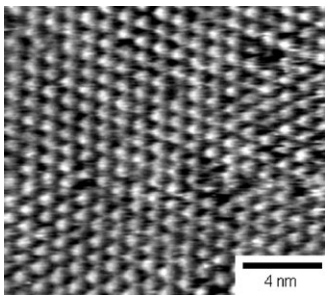

Fig. 1 STM image of an adsorbed fullerene monolayer on Au(111).

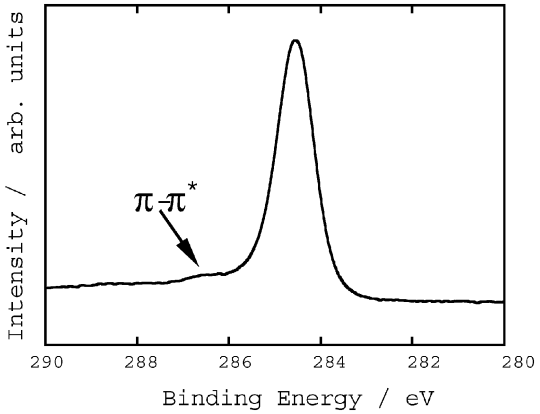

Fig. 2 XPS spectrum for the C (1*s*) core level of fullerene adsorbed on Au(111) referred to the Au ($4f_{7/2}$) peak (84.0 eV) for a clean Au surface. The position of the π–π* shake-up peak is indicated.

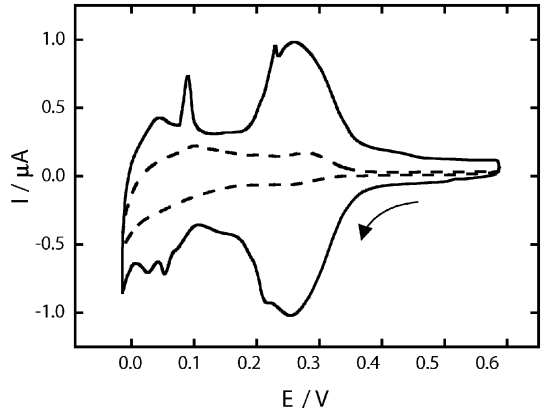

Fig. 4 Cyclic voltammetry for Cu UPD on a polycrystalline Au bead in 0.05 M H_2SO_4 + 1 mM $CuSO_4$; sweep rate = 5 mV s^{-1}, with (dashed line) and without (solid line) an adsorbed fullerene monolayer.

(111) surface was 440 μC cm^{-2}.[38] This represents the total charge required for the deposition of a fully discharged monolayer of Cu as calculated from the surface atom density of a Au(111) surface. The results obtained indicate the absence of adsorbed impurities and a coverage of more than 90% of the Au surface was determined.[13] The measurements on single crystal surfaces were carried out in order to image the structure of the adsorbed fullerene monolayer. As will be discussed later, the voids present within the film are the environment where the ORR takes place on the nanostructured surface.

Fig. 2 shows the XPS spectrum for the C1*s* core level of a fullerene monolayer adsorbed on Au(111). A downward shift of the binding energy of 0.5 eV for the C1*s* core level (284.5 eV) with respect to that of bulk fullerene (285.0 eV[39]) was observed. Similar results have been obtained for other metal surfaces such as Cu and Pt, with a decrease in the binding energy of 0.5 and 0.4 eV, respectively.[40,41] It has been proposed that the shift of the C1*s* peak results from charge transfer from the metal substrate to the adsorbate.[41] The shift varied with the substrate material and its crystal structure and with the thickness of the fullerene overlayers. In addition, a small peak at 286.4 eV is also observed due to π–π* transitions.[42] This band, displaced by 1.9 eV with respect to the C1*s* peak, has been attributed to a shake-up process involving direct excitation across the π–π* gap.[42] Although there is good evidence for charge transfer from the metal to fullerene,[12] the strong interactions responsible for adsorption are not only electrostatic but display a strong covalent character.[42–44] Other surface orientations show a similar strong adsorption of fullerene as that observed for Au (111). Fig. 3 shows an STM image of fullerene adsorbed on Au(100). Hexagonal close packing is observed, with a spacing of 0.99 ± 0.03 nm between neighbours, in good agreement with the results for Au(111). Coverage determined from the Cu UPD charge gave a value similar to that for Au(111). Previous STM and Cu UPD measurements showed that similar close packed, high coverage, fullerene layers were formed for stepped Au surfaces.[13]

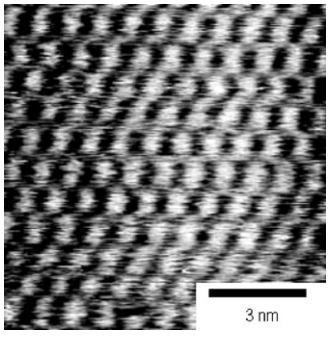

Fig. 3 STM image of an adsorbed fullerene monolayer on Au(100).

Fig. 4 shows a similar behaviour for polycrystalline gold (poly-Au). This figure compares the cyclic voltammetry for Cu UPD on bare Au and on the same electrode modified with a monolayer of attached fullerene. From the Cu UPD charge, a coverage of 88% of the active surface is estimated. Thus, the results obtained for both low and high Au index planes and for poly-Au demonstrate that the fullerene overlayers show a high adaptability to the structure of the underlying substrate and very high monolayer coverages are obtained regardless of the crystallographic structure of the metal surface.

3.2. Oxygen reduction on bare poly-Au

In order to investigate the electrocatalytic properties of fullerene the ORR was studied in the absence and presence of an adsorbed fullerene monolayer. A blank measurement was carried out by immersing the Au RDE in the distilled toluene used to make the fullerene solution to ascertain the absence of adsorbable impurities. No significant difference in the voltammograms was observed compared to the original Au surface showing that the effects observed are not caused by the adsorption of adventitious impurities. Fig. 5 shows linear sweep voltammograms for oxygen reduction in 0.1 mol dm^{-3} KOH on a bare poly-Au RDE at different rotation rates (ω). For Au in alkaline solutions, the potential dependence of the current and the reaction mechanism is based significantly on surface crystallography. Note the presence of a current peak at −0.3 V, which is related to (100) sites where oxygen is reduced to water following a four-electron transfer process.[24,25] It has been proposed that this behaviour is related to the involvement of $AuOH^{-(1-\lambda)}$ surface species that act as electrocatalytic centres for the four electron reduction pathway. The decrease in coverage by these species as the potential is made more negative leads to the observed current decrease when the reaction changes from a $4e^-$ to a $2e^-$ mechanism. The difference in activity, however, was independent of pH, thus suggesting that HO_2^- adsorption plays a key role in this reaction.[26]

The measurements were highly reproducible and similar to those previously reported.[20,22] The rotation rate dependence of the current was analysed using the Koutecky–Levich equation:[2]

$$\frac{1}{j} = \frac{1}{j_k} - \frac{1}{0.62nFD^{2/3}\nu^{-1/6}c^b\omega^{1/2}} \qquad (1)$$

where j is the current density, F is the Faraday constant, n is the number of electrons transferred per oxygen molecule, D is the diffusion coefficient (1.73×10^{-5} cm^{-2} s^{-1} [45]), ν is the kinematic viscosity of the solution (0.01 cm^2 s^{-1} [2]), c^b is the bulk

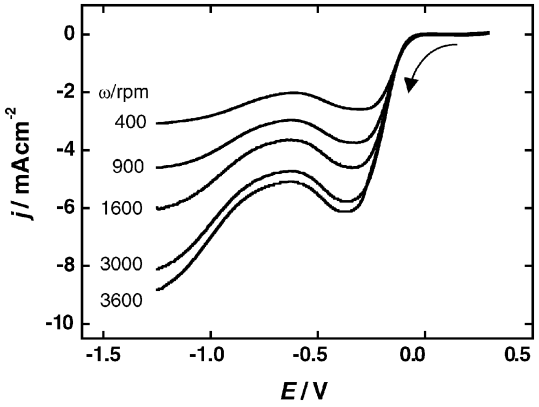

Fig. 5 Linear sweep voltammograms for oxygen reduction on a bare polycrystalline Au RDE surface in oxygen saturated 0.10 M KOH. Scan rate: 10 mV s^{-1}; rotation rates: 400, 900, 1600, 3000 and 3600 rpm.

concentration of dissolved oxygen (1.29×10^{-6} mol cm^{-3} [39]) and j_k is the kinetic current density for $\omega \rightarrow \infty$. A linear dependence of the reciprocal of the current density on $\omega^{-1/2}$ was observed in a wide potential range (Fig. 6). In the mixed kinetic-diffusion potential region, an intercept in the Koutecky–Levich plots is observed due to the kinetics of the reaction. n was obtained from the slope of these plots [eqn. (1)] and its potential dependence is shown in the inset of Fig. 6. n reaches a minimum close to 3 for $E \sim -0.6$ V, indicating partial reduction of oxygen to peroxide. The increase of n at more positive potentials is related to the presence of Au(100) domains, where oxygen is reduced to water. At very large overpotentials (more negative than −1.0 V), the value of n increases to 4, as previously observed.[25]

3.3. Oxygen reduction on fullerene modified poly-Au

No electrochemical activity was observed for adsorbed fullerene in the absence of O_2 between 0 and −1.3 V (Data not shown). Fig. 7 shows that the reduction of oxygen on a fullerene modified poly-Au RDE is strongly inhibited between –0.1 and –0.4 V. The corresponding Koutecky–Levich plots and the potential dependence of n are shown in Fig. 8. Importantly, n is close to 2 at -0.4 V $< E <$ -0.75 V indicating a change in mechanism caused by the presence of

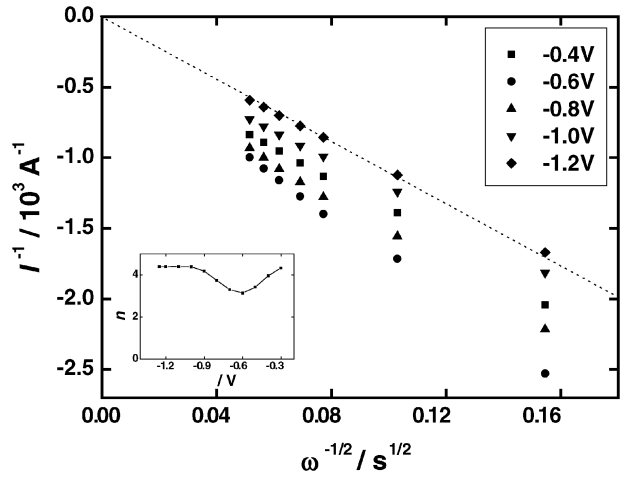

Fig. 6 Koutecky–Levich plots for oxygen reduction on a bare Au RDE obtained from Fig. 5. The dotted line represents $j^{-1} = (1/0.62nFc^{b}D^{2/3}\nu^{-1/6})\ \omega^{-1/2}$ for $n = 4$. Inset: dependence of the number of electron transferred per oxygen molecule on a bare Au RDE on potential; values calculated from the slope of the corresponding Koutecky–Levich plots.

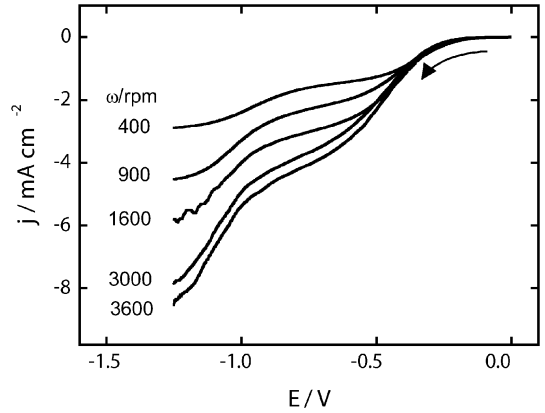

Fig. 7 Linear sweep voltammograms of oxygen reduction on a fullerene modified Au RDE surface in oxygen saturated 0.10 M KOH. Scan rate: 10 mV s^{-1}; rotation rates: 400, 900, 1600, 3000 and 3600 rpm. The results shown correspond to the first scan for each rotation rate.

the adsorbed fullerene layer (compare with Fig. 6). At potentials more negative than −0.75 V, n increases and finally approaches a value of 4 at −1.0 V. The adsorbed fullerene films were stable between 0.3 and −0.75 V since no change in the ORR voltammograms was observed in this potential range after several scans. However, when the potential sweeps were extended to −1.25 V, significant differences in the voltammograms after cycling the potential were apparent (Fig. 9). A negative shift of *ca.* 300 mV for the onset of oxygen reduction was observed after the first scan. The reduction rate increased in the whole potential range with the number of sweeps, indicating desorption of fullerene at potentials more negative than −0.75 V and resulting in the recovery of the current corresponding to bare Au. For each of the experiments shown in Fig. 7, the electrode surface was repolished and a new monolayer of fullerene attached before measurement.

A comparison of the results for a fullerene covered surface with those for a bare Au electrode is shown in Fig. 10, clearly demonstrating that fullerene is desorbed at potentials more negative than −0.75 V. As this layer is desorbed, the value of n increases to that corresponding to a bare Au electrode. The strong potential dependence of the rate of oxygen reduction in this potential range is a consequence of the change of n from two to four resulting from both the desorption of fullerene and the change in reduction mechanism on bare Au at negative potentials (see Fig. 6). It can be concluded that fullerene does not display any catalytic activity towards oxygen reduction but

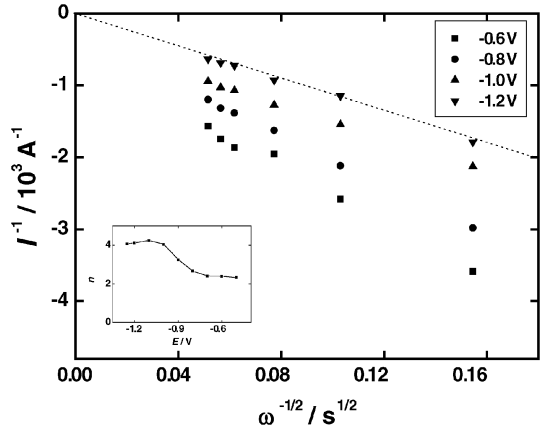

Fig. 8 Koutecky–Levich plots for oxygen reduction on a fullerene modified Au RDE obtained from the results shown in Fig. 7. The dotted line represents $j^{-1} = (1/0.62nFc^{b}D^{2/3}\nu^{-1/6})\ \omega^{-1/2}$ for $n = 4$. Inset: dependence of n on potential for a fullerene modified Au RDE calculated from the slope of the corresponding Koutecky–Levich plots.

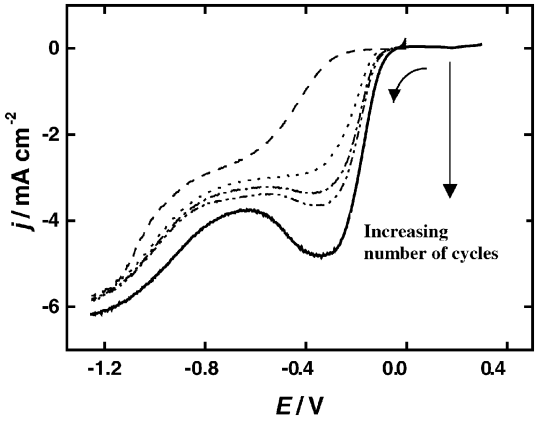

Fig. 9 Linear sweep voltammograms for oxygen reduction on a fullerene modified electrode in oxygen saturated 0.10 M KOH after different number of cycles between 0.3 and −1.25 V. Scan rate: 10 mV s^{-1}; rotation rate: 1600 rpm. From top to bottom, Au/C_{60}, 1st scan; Au/C_{60}, 2nd scan; Au/C_{60}, 5th scan; Au/C_{60}, 10th scan; bare poly-Au.

rather acts as an inert material strongly adsorbed to the metal, creating an interfacial structure that lowers specifically the rate of reduction of oxygen to water. The inhibition of electron transfer reactions by fullerene thick films in aqueous electrolytes has previously been reported and the present results are in broad agreement with these previous observations.[16,18] The main difference is that in the present case, the electrodes used had monolayer coverage by fullerene, which may account for the onset of desorption at a more positive potential than previously observed.[17]

3.4. Influence of adsorbed fullerene on the mechanism of oxygen reduction

The results above show that the adsorption of fullerene has a profound effect on the mechanism of O_2 reduction that is not simply a blocking effect. Adsorbed fullerene can affect the reaction kinetics in two ways, by altering the reaction environment and/or by blocking specific reaction sites. For the first case, it is proposed that the strong specific adsorption of fullerene leads to the formation of a region of high local hydrophobicity by displacement of water molecules from the surface, thus inhibiting their participation in the reaction. The high coverage changes the reaction site by providing a partially water deficient (aprotic) environment due to a lack of space for the inclusion of water molecules in the reaction region. In addition, the dielectric properties of water present in the confined interstitial regions between fullerene molecules would correspond to that of a polar, non-hydrogen bonded organic solvent.

In aprotic media, oxygen is reduced to superoxide according to:

$$O_2 + e^- \rightarrow O_2^{\bullet -} \qquad \text{(III)}$$

The stability of $O_2^{\bullet -}$ in organic solvents is well known.[46,47] The formation of superoxide has also been observed in aqueous alkaline solutions in the presence of strongly adsorbed surfactants[46] demonstrating the importance of adsorbates in the O_2 reduction mechanism. The first electron transfer step [reaction (III)] is followed either by proton transfer and heterogeneous reduction of superoxide:

$$O_2^{\bullet -} + H_2O \rightarrow HO_2^{\bullet} + OH^- \qquad \text{(IV)}$$

$$HO_2^{\bullet} + e^- \rightarrow HO_2^- \qquad \text{(V)}$$

i.e., an ECE mechanism, or by its chemical disproportionation:[47]

$$2O_2^{\bullet -} + H_2O \rightarrow O_2 + O_2H^- + OH^- \qquad \text{(VI)}$$

Both reaction sequences require water. The total number of electrons transferred per oxygen molecule will therefore be less than 4 and the reaction occurring within the confined environment produced by the adsorbed fullerene molecules can lead to the formation of peroxide. Changes in reaction mechanism of electrochemical reactions due to the displacement of water by organic adsorbates are well-documented and constitute, for example, the basis for the industrial synthesis of adiponitrile by the electrodimerisation of acrylonitrile.[48]

Besides the change of solvent properties in the interfacial region, the decrease of both the current density and n at $E > -0.8$ V by adsorbed fullerene (Figs. 8 and 10) can also be related to the blocking effect of the adsorbed layer. For this to be effective in switching the reaction from a $4e^-$ to a $2e^-$ process the adlayer should suppress the bridge adsorption of oxygen on Au (Yeager and Griffith models), limiting adsorption of oxygen to that corresponding to end-on coordination (Pauling model). This type of blocking is the so-call third body effect.[49] Fig. 11 shows a schematic representation of the proposed steric effects. Fig. 11a and 11b show the oxygen molecules bridged between two nearest neighbour Au atoms in the absence of the fullerene overlayer, while Figs. 11c and 11d show the preferred end-on configuration of adsorbed oxygen in

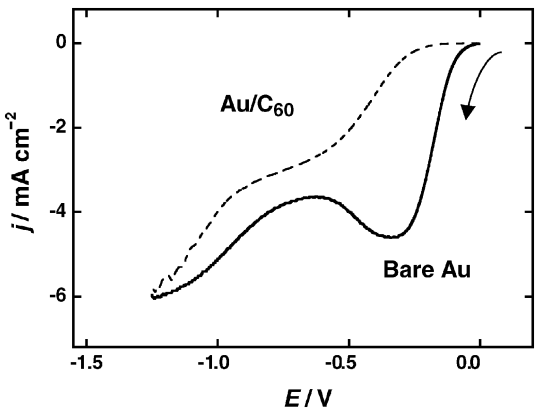

Fig. 10 Comparison of linear sweep voltammograms for oxygen reduction on a rotating disk bare poly-Au electrode and the same electrode modified with a monolayer of fullerene. Rotation rate = 1600 rpm; sweep rate = 10 mV s^{-1}.

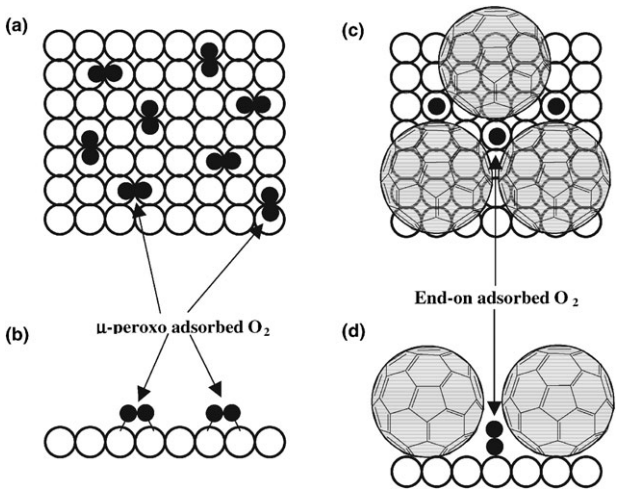

Fig. 11 Schematic diagram illustrating the proposed changes in adsorption configuration for adsorbed oxygen resulting from the attachment of the electrochemically "silent" fullerene molecules; (a) μ-peroxo adsorption of oxygen on bare Au, top view; (b) side view of (a); (c) change of coordination of adsorbed oxygen from μ-peroxo to end-on caused by the attachment of fullerene to the gold surface; top view; (d) side view of (c).

the confined space at the surface caused by the presence of the fullerene monolayer. At negative potentials, partial desorption of fullerene molecules frees adsorption sites for μ-peroxo and side-on coordination for the oxygen molecules, thus resulting in an increase in the contribution from the four-electron reduction pathway.

Similar changes in reduction mechanism have been reported for Cu and bromide adsorption on Pt[50,51] when the coordination geometry of oxygen is imposed by the adlayer structure. Itaya *et al.*[50] demonstrated the inhibition of the four-electron reduction process caused by the underpotential deposition of Cu on Pt. The honeycomb structure of UPD Cu formed in the potential range between the two sets of peaks characteristic of Cu UPD inhibited bridge μ-peroxo coordination between nearest-neighbour Pt atoms, therefore restricting O_2 adsorption to an end-on geometry, thus enhancing the rate of formation of hydrogen peroxide. Another example of changes in reduction mechanism caused by changes in surface coordination is that produced by hydrogen UPD (H UPD). Markovic *et al.*[52] showed that the four-electron reduction of oxygen was switched to a two-electron pathway when the Pt surface is covered by adsorbed hydrogen that forces a change of oxygen adsorption geometry from μ-peroxo to end-on.

For a complex reaction such as oxygen reduction, surface structure and in particular, confinement effects can play a major role in controlling the mechanism. For fullerene, STM images show the presence of hollow sites in the adsorbed layer (Figs. 1 and 3). From simple geometrical considerations, the diameter of the available hollow sites is approximately 0.45 nm, assuming a fullerene diameter of 0.7 nm and considering a measured separation between adsorbed molecules of 1.0 nm. This diameter has to be compared with the hard sphere diameter of an oxygen molecule, of 0.346 nm.[53] Although this is a rough estimate, it clearly demonstrates that there is not adequate space for a bridge type adsorption of oxygen in the hollow sites of the adsorbed films. These steric considerations (see cartoons in Fig. 11) should make more favourable the selective end-on adsorption of oxygen molecules at the fullerene modified surfaces with the corresponding inhibition of the four-electron reduction pathway. Fullerene represents, in this case, an inert material and in the context of oxygen reduction, it is electrochemically inactive. In spite of its inertness, this is an interesting example of how the course of electrocatalytic reactions can be profoundly altered by the specific blocking of surface sites.

4. Summary

The importance of this research is to have demonstrated that: (1) fullerene is electrochemically inert as an electrocatalytic material for oxygen reduction, and (2) geometrical constraints resulting from its adsorption alter the mechanism of electrocatalytic reactions by the specific blocking of active sites.

The oxygen reduction reaction was investigated on Au surfaces that had been modified with adsorbed fullerene monolayers to determine their influence in the oxygen reduction mechanism. Fullerene adsorbed on Au forms a close packed film with strong interaction between the fullerene molecules and the Au substrate. Fullerene represents an electrochemically inert material for oxygen reduction and can change both the properties of the nanoscale domains where electron transfer takes place to create a local hydrophobic environment by inhibiting the participation of water molecules in the reaction. In addition, the adsorption of fullerene leads to the specific blocking of surface sites, inhibiting the side-on coordination of oxygen. It is proposed that these two effects result in the selective reduction of oxygen to hydrogen peroxide on gold modified with adsorbed fullerene.

Acknowledgements

The research was supported by the European Union CLETEPEG project (Contract No. G5RD-CT-2001-00463). A.K. gratefully acknowledges the award of an Overseas Research Students Scholarship, UK. Useful comments on the properties of adsorbed fullerene by Prof. I. Panas, Chalmers University of Technology, Göteborg, and help with the XPS measurements by Dr G. Beamson, Daresbury, are gratefully acknowledged.

References

1 A. Wieckowski, in *Interfacial Electrochemistry: Theory, Experiment and Applications*, Marcel Dekker, New York, 1999, pp. 631–647.
2 K. Tammeveski, K. Kontturi, R. J. Nichols, R. J. Potter and D. J. Schiffrin, *J. Electroanal. Chem.*, 2001, **515**, 101–112.
3 M. T. McDermott, C. A. McDermott and R. L. McCreery, *Anal. Chem.*, 1993, **65**, 937–944.
4 R. L. McCreery, K. K. Cline, C. A. McDermott and M. T. McDermott, *Colloid Surf., A*, 1994, **93**, 211–219.
5 H. W. Kroto, J. R. Heath, S. C. O'Brien, R. F. Curl and R. E. Smalley, *Nature (London)*, 1985, **318**, 162–163.
6 C. Jehoulet, Y. S. Obeng, Y. T. Kim, F. Zhou and A. J. Bard, *J. Am. Chem. Soc.*, 1992, **114**, 4237–4247.
7 P. M. Allemand, *Science*, 1991, **253**, 301–303.
8 A. F. Hebard, M. J. Rosseinsky, R. C. Haddon, D. W. Murphy, S. H. Glarum, T. T. Palstra, A. P. Ramirez and A. R. Kortan, *Nature (London)*, 1991, **350**, 600–601.
9 E. I. Altman and R. J. Colton, *Surf. Sci.*, 1992, **279**, 49–67.
10 E. I. Altman and R. J. Colton, *Surf. Sci.*, 1993, **295**, 13–33.
11 J. K. Gimzewski, S. Modesti, Ch. Gerber and R. R. Schlittler, *Chem. Phys. Lett.*, 1993, **213**, 401–406.
12 T. Sakurai, X. D. Wang, Q. K. Xue, Y. Hasegawa, T. Hashizume and H. Shinohara, *Prog. Surf. Sci.*, 1996, **51**, 263–408.
13 A. Kuzume, E. Herrero, J. M. Feliu, R. J. Nichols and D. J. Schiffrin, *Phys. Chem. Chem. Phys.*, 2004, **6**, 619–625.
14 Á. Szűcs, A. Loix, J. B. Nagy and L. Lamberts, *J. Electroanal. Chem.*, 1995, **397**, 191–203.
15 Á. Szűcs, A. Loix, J. B. Nagy and L. Lamberts, *J. Electroanal. Chem.*, 1996, **402**, 137–148.
16 Á. Szűcs, M. Tölgyesi, M. Novák, J. B. Nagy and L. Lamberts, *J. Electroanal. Chem.*, 1996, **419**, 39–46.
17 P. Janda, T. Krieg and L. Dunsch, *Adv. Mater.*, 1998, **10**, 1434–1438.
18 M. Csiszár, Á. Szűcs, M. Tölgyesi, Á. Mechler, J. B. Nagy and M. Novák, *J. Electroanal. Chem.*, 2001, **497**, 69–74.
19 R. G. Compton, R. A. Spackman, D. J. Riley, R. G. Wellington, J. C. Eklund, A. C. Fisher, M. L. H. Green, R. E. Doothwaite, A. H. H. Stephens and J. Turner, *J. Electroanal. Chem.*, 1993, **344**, 235–247.
20 H. S. Wroblowa, Y. C. Pan and G. Razumney, *J. Electroanal. Chem.*, 1976, **69**, 195–201.
21 A. J. Appleby and M. Savy, *J. Electroanal. Chem.*, 1978, **92**, 15–30.
22 P. Fischer and J. Heitbaum, *J. Electroanal. Chem.*, 1980, **112**, 231–238.
23 R. R. Adzic, N.M. Markovic and V. B. Vesovic, *J. Electroanal. Chem.*, 1984, **165**, 105–120.
24 N. M. Markovic, R. R. Adzic and V. B. Vesovic, *J. Electroanal. Chem.*, 1984, **165**, 121–133.
25 S. Strbac and R. R. Adzic, *J. Electroanal. Chem.*, 1996, **403**, 169–181.
26 A. Prieto, J. Hernandez, E. Herrero and J. M. Feliu, *J. Solid State Electrochem.*, 2003, **7**, 599–606.
27 R. Adzic, in *Electrocatalysis*, ed. J. Lipkowski and P. N. Ross, Wiley-VCH, Inc., Weinheim, 1998.
28 E. B. Yeager, *Electrochim. Acta*, 1984, **29**, 1527–1537.
29 A. W. E. Chan, R. Hoffmann and W. Ho, *Langmuir*, 1992, **8**, 1111–1119.
30 *Structural Effects in Electrocatalysis and Oxygen Electrochemistry*, ed. E. Yeager, M. Razaq, D. Gervasio, A. Razaq and D. Tryk, The Electrochemical Society Inc., Pennington, NJ, 1992, PV 92-11, p. 440.
31 J. Clavilier, D. Armand, S. G. Sun and M. Petit, *J. Electroanal. Chem.*, 1986, **241**, 267–277.
32 C. J. Yang and S. A. Jenekhe, *Chem. Mater.*, 1995, **7**, 1276–1285.
33 R. Greef, *ELLGRAPH fitting software*, Optochem, Southampton, 1992.

34 S. Uemura, A. Ohira, T. Ishizaki, M. Sakata, M. Kunitake, I. Taniguchi and C. Hirayama, *Chem. Lett*., 1999, 279–280.
35 S. Uemura, M. Sakata, I. Taniguchi, M. Kunitake and C. Hirayama, *Langmuir*, 2000, **17**, 5–7.
36 S. Uemura, P. Samori, M. Kunitake, C. Hirayama and J. P. Rabe, *J. Mater. Chem*., 2002, **12**, 3366–3367.
37 A. Kuzume, E. Herrero, J. M. Feliu, R. J. Nichols and D. J. Schiffrin, *J. Electroanal. Chem*., 2004, **570**, 157–161.
38 E. Herrero, L. J. Buller and H. D. Abruña, *Chem. Rev*., 2001, **101**, 1897–1930.
39 P. Reinke and P. Oelhafen, *J. Chem. Phys*., 2002, **116**, 9850–9855.
40 J. E. Rowe, P. Rudolf, L. H. Tjeng, R. A. Malic, G. Meigs, C. T. Chen, J. Chen and E. W. Plummer, *Int. J. Mod. Phys. B*, 1992, **6**, 3909.
41 N. Swami, H. He and B. E. Koel, *Phys. Rev. B*, 1999, **59**, 8283–8291.
42 A. J. Maxwell, P. A. Bruhwiler, A. Nilsson and N. Martensson, *Phys. Rev. B*, 1994, **49**, 10717–10725.
43 T. R. Ohno, Y. Chen, S. E. Harvey, G. H. Kroll, J. H Weaver, R. E. Haufler and R. E. Smalley, *Phys. Rev. B*, 1991, **44**, 13747–13755.
44 L. L. Wang and H. P. Cheng, *Phys. Rev. B*, 2004, **69**, 165417.
45 E. Ahlberg, F. Falkenberg, J. A. Manzanares and D. J. Schiffrin, *J. Electroanal. Chem*., 2003, **548**, 85–94.
46 J. Chevalet, F. Rouelle, L. Gierst and J. P. Lambert, *J. Electroanal. Chem*., 1972, **39**, 201–216.
47 J. Divisek and B. Kastening, *J. Electroanal. Chem*., 1975, **65**, 603–621.
48 D. Pletcher and F. C. Walsh, in *Industrial Electrochemistry*, Blackie Academic & Professional, London, 1993, ch. 6.
49 E. Herrero, A. F. Vega, J. M. Feliu and A. Aldaz, *J. Electroanal. Chem*., 1993, **350**, 73–88.
50 T. Abe, G. M. Swain, K. Sashikata and K. Itaya, *J. Electroanal. Chem*., 1995, **382**, 73–83.
51 J. X. Wang, N. S. Marinkovic and R. R. Adzic, *Colloids Surf., A*, 1998, **134**, 165–171.
52 N. M. Markovic, H. A. Gasteiger and P. N. Ross Jr, *J. Phys. Chem*., 1995, **99**, 3411–3415.
53 S. K. Shoor and K. E. Gubbins, *J. Phys. Chem*., 1969, **73**, 498–505.